Benchmarking TD-DFT against vibrationally-resolved absorption spectra at room temperature: 7-aminocoumarins as test cases.

Francesco Muniz-Miranda,[a] Alfonso Pedone,[,a] Giulia Battistelli,[b] Marco Montalti,[b] Julien Bloino,*[c,d] Vincenzo Barone.[d]*

(a) Dipartimento di Scienze Chimiche e Geologiche, Università di Modena e Reggio Emilia, via G. Campi 183, Modena, 41125, Italy.

(b) Dipartimento "G. Ciamician", Università di Bologna, Bologna,40126, Italy.

(c) Consiglio Nazionale delle Ricerche, Istituto di Chimica dei Composti OrganoMetallici (ICCOM-CNR), UOS di Pisa, Area della Ricerca, via G. Moruzzi 1, Pisa, 56124, Italy

(d) Scuola Normale Superiore di Pisa, Piazza dei Cavalieri 7, Pisa, 56126, Italy.

Corresponding Authors

*Dr. Alfonso Pedone, Dipartimento di Scienze Chimiche e Geologiche, Università di Modena e Reggio Emilia, via G. Campi 103, Modena, 41125, Italia. Email: alfonso.pedone@unimore.it; Dr. Julien Bloino, Consiglio Nazionale delle Ricerche, Istituto di Chimica dei Composti Organo-Metallici (ICCOM-CNR), UOS di Pisa, Area della Ricerca, via G. Moruzzi 1, Pisa, 56124, Italy. Email: julien.bloino@pi.iccom.cnr.it

Abstract

Time-dependent density functional theory (TD-DFT) is usually benchmarked by evaluating how the vertical excitation energies computed by using different exchange-correlation (XC) functionals compare with the maximum of the absorption spectra. However, the latter does not necessarily coincide with the vertical energies because it is affected by the vibronic band structure that has to be properly accounted for.

In this work, we have evaluated the performance of several functionals belonging to different families in reproducing the vibronic structure (band shape) of four 7-aminocoumarin molecules of technological interest, whose spectra have been recorded in methylcyclohexane and acetonitrile solvents. In order to compare in the more consistent way the computed vibronic spectra with the experimental ones, the effect of the temperature, often neglected, was also taken into account. We have found that no single functional provides simultaneously accurate band positions and shapes, but the combination of ωB97X vibronic couplings with PBE0 vertical energies can lead to very satisfactory results.

In addition to the assessment of XC functionals, several adiabatic and vertical models proposed in the literature to compute vibrationally resolved electronic spectra have been tested and validated with respect to experiments. On these grounds, the adiabatic Hessian model has been used to perform a complete analysis of the ωB97X/PBE0 vibronic transitions contributing to the final band shapes of the investigated aminocoumarin molecules.

Introduction

Nowadays, density functional theory (DFT)[1] and its time-dependent extension (TD-DFT)[2,3] are the most widely employed quantum mechanical (QM) tools for modeling a large number of ground- and excited-state properties of medium-to-large molecular systems in various environments.[4–11] The popularity of DFT and TD-DFT is mainly due to the favourable performance-to-accuracy ratio and to the ongoing development of a wide variety of increasingly complex and accurate exchange-correlation (XC) functionals.

Concerning the calculation of absorption/emission energies, several past investigations have shown that the local density approximation (LDA) strongly underestimates vertical excitation energies (VEEs) of most organic molecules, whereas better estimations are obtained by using the generalized gradient approximations (GGAs) or the so-called meta-GGA approaches, which include also the density Laplacian.[8,12,13] The most accurate UV-vis spectra are usually computed by using global hybrid functionals (GHs), such as PBE0[14] or B3LYP[15], which explicitly include a constant fraction of Hartree-Fock (HF) exchange. However, GHs still have limitations deriving from the fact that the density is not influenced by a change in the nearby electronic distribution[16–18] and thus van der Waals forces,[19–21] bond length alternation in semiconducting polymers,[22] nonlinear optics properties of long π-conjugated chains,[16] Rydberg and charge-transfer (CT) electronic states are not well reproduced.[17,23]

Thanks to the developments of range-separated hybrid (RSH)[24–30] functionals, which use a growing fraction of exact exchange as the inter-electronic distance increases and of the so-called double-hybrids (DH) functionals, which include also a second-order perturbative evaluation of non-local terms involving virtual orbitals,[31] most of the aforementioned deficiencies can be overcome. However, the complexity of RSHs, often involving several additional parameters, and the computational cost of DHs, give rise to new issues and their applicability to a given case needs to be

carefully assessed. In general, the multitude of available exchange-correlation functionals raises the issue of carefully choosing the most suitable one for the system and/or property of interest.

For instance, the performance of TDDFT on the reproduction of vertical and adiabatic energies of valence transitions has been extensively studied and a very large number of benchmarks have been published in the last decade.[13,23,32–34] These investigations have shown that the expected TD-DFT accuracy is strongly dependent on the nature of the considered state (n→π*/π→π*, singlet or triplet states) and the functional. For low-lying singlet transitions the average deviations often remain within 0.2–0.3 eV when using typical hybrid functionals, such as B3LYP[15] or PBE0,[14,35] an error that could even be decreased with DH functionals. RSH functionals relying on a relatively soft attenuation, e.g. CAM-B3LYP[29] and ωB97XD,[36] or the different functionals of the Minnesota family, such as the M05-2X,[37] M06-2X[38] and M08-HX[39] deliver relatively small errors for CT states without significantly degrading the accuracy of local states.[8,10,12,40,41]

However, it is worth pointing out that absorption or emission band maxima of experimental spectra do not necessarily coincide with vertical energies, and it is necessary to properly take into account the vibronic structure. [42–44] With the growing availability of packages able to compute efficiently vibronic transitions, the proper assessment of the performance of XC functionals against vertical excitation energies (VEEs) is no longer sufficient and future computational efforts should be devoted to the reproduction of the vibronic structure (band shape) of electronic spectra in order to gain more detailed and accurate information on the potential energy surfaces (PES) of organic molecules.

Dierksen and Grimme[45] performed the first systematic work along this direction in 2004; they computed the band structure of a large set of aromatic molecules in the gas phase by using three functionals and showed that functionals with 30-50% of HF exchange reproduced well the experimental band shape. More recently, Stendardo *et al.*[46] showed that the CAM-B3LYP and PBE0 functionals reproduce the vibrational structure of the absorption spectra of dithiophene molecules better than BLYP, BHLYP and B3LYP. Jacquemin and coworkers[47] evaluated the performance of 18

functionals belonging to different families in reproducing the vibronic couplings of anthraquinone derivatives in solution concluding that no single functional simultaneously provides highly accurate positions and intensities of the different bands, but ωB97XD provided the best overall results.

However, in all these studies the vibronic spectra computed at 0K were compared to the experimental counterparts collected at room temperature. Temperature effects are then assumed to have an inhomogeneous broadening effect which can be accounted for by applying Gaussian distribution functions with proper half-widths at half-maximum to the stick spectrum obtained at T=0K. However, as the contributions of hot-bands become more important, this approximation may become too rough and an explicit computation of temperature effects is necessary. For this reason, when dealing with experiments at room or higher temperature, a preliminary evaluation of the actual effects of the temperature can be useful when defining the computational protocol.

In this work we benchmarked several global hybrid and range separated XC functionals based on the vibrationally-resolved absorption spectra of four 7-aminocoumarin molecules, reported in Figure 1, which are widely used as laser dyes in the blue-green region[48,49] and studied for their applicability as organic semiconductors, optical memory materials and optical sensors when conjugated to polymeric thin films[50] or encapsulated in silica matrix.[41,51] All calculations were carried out with the module written by some of us to compute efficiently vibronic spectra within the time-independent (TI)[52] and time-dependent (TD)[53] frameworks within a widespread quantum chemical package.[54] For the reasons explained above and at variance with most earlier studies, temperature effects were also included in all calculations in order to compare in the most consistent way the computed spectra with their experimental counterparts recorded in methyl-cyclohexane and acetonitrile and reported in this manuscript for the first time.

The paper is organized as follows. In Sections 2.1, 2.2 and 2.3, we describe in sequence the experimental details, the computational strategy employed to simulate vibronic spectra and the functionals, basis sets and approximations employed in all calculations. In Section 3.1, we investigate

the performance of 8 functionals (belonging to different families) in reproducing the band-shapes of the absorption spectra for the four investigated coumarin molecules. In Section 3.2 we compare several models to compute the vibronic spectra, based on slightly different descriptions of the final-state PES, whereas an in-depth analysis of the vibronic transitions for these specific dyes is given in Section 3.3.

Methods

2.1 Experimental details.

All reagents and solvents were acquired from Sigma Aldrich and used as received without further purification. UV-visible absorbance spectra were recorded at room temperature on solutions of the four molecules investigated of concentration $3 \cdot 10^{-5}$M. A Perkin Elmer Lambda 650 spectrophotometer with a quartz cells with 1.0 cm path length was used.

2.2 Computational strategies for vibrationally resolved absorption spectra.

The line-shape of the one-photon absorption (OPA) spectra in the TI framework[52] was computed from the formula:

$$\sigma(\omega)_{abs} = \frac{4\pi^2\omega}{3c} \sum_i \rho_i \sum_f \left|\langle \Psi_i | \hat{\boldsymbol{\mu}} | \Psi_f \rangle\right|^2 \delta(E_f - E_i - \hbar\omega) \qquad (1)$$

Where ρ_i is the Boltzmann population of initial molecular state i and $\sigma(\omega)$ is the rate of photon absorption per molecule and per unit of radiant energy for an incident photon of energy $\hbar\omega$. Ψ_i and Ψ_f represent the molecular wave functions of the initial and final states, respectively, and $\boldsymbol{\mu}$ is the electric dipole. The Dirac function δ is in practice replaced by a distribution function to simulate the broadening observed experimentally.

In most cases, the electronic states involved in the transitions observed in the electronic spectra are assumed sufficiently separated from each other so that the summations can be done by considering only two electronic states at a time (the initial and final ones). Spectra involving multiple transitions

are then obtained by summing the band-shape calculated for each single electronic transition. At the same time, the Born-Oppenheimer approximation is employed so that the nuclear and electronic wave functions are uncoupled and the vibronic transitions are computed from overlap integrals between vibrational states of the initial and final electronic states. The complete derivation can be found in Refs.[44,52,55,56] and will not be repeated here. However, in order to understand the models at our disposal to define different computational protocols for the simulation of vibronic spectra, a short discussion of some key aspects can be useful.

First, since we are interested in the vibrational contributions to the electronic spectra and in order to compute the overlap integrals, a representation of the PESs of the two electronic states involved in the transition is needed. Except for the smallest systems, this is done at a purely harmonic level. As the molecular systems generally undergo structural changes upon the electronic excitation, the minima of the PESs are not superimposed. As a result, the region corresponding to the vertical transition, the so-called Franck-Condon (FC) region, with the highest overlap, can be poorly represented by the harmonic final-state PES computed about its minimum. At variance, the harmonic PES computed in the FC region can reproduce poorly the PES about its minimum. Hence, two strategies can be devised, which differ by the description of the final-state PES, the initial-state one being always computed about its minimum. In the adiabatic model, referred to as Adiabatic Hessian (AH) in the following, the PES of the final state is computed about its minimum, so that both initial and final states are treated in the same way. On the contrary, in the vertical model (Vertical Hessian, VH), the final-state PES is computed in the FC region, that is about the initial-state equilibrium geometry. In practice, VH will be more accurate to represent the most intense transitions at the expense of an approximation of the frequencies in the final states, leading to a lower precision in the band positions. On the contrary, AH will describe more precisely the fine structure of the spectrum and the band position but the reliability of the most intense transitions will depend on the shift between the respective PES (the smaller, the more accurate). Indeed, VH and AH are equivalent if both PES are superposed, that is to say their respective minima are vertically aligned. As a final

remark, due to the computational cost of excited-state PESs, cheaper approaches have been proposed where the final-state PES is assumed equal to the initial-state one. Those approximated models are called adiabatic shift (AS) for the adiabatic model, and vertical gradient (VG, also known as the linear coupling model)[57] for the vertical one.[57] Except for the calculation of the Duschinsky matrix and shift vector, presented below, the machinery for the calculation of the overlap integrals is the same, irrespective of the chosen model (vertical or adiabatic).

Another important point is the approximation used for the definition of the transition dipole moment, $\boldsymbol{\mu}_{if}^{e} = \langle \phi_i | \hat{\boldsymbol{\mu}} | \phi_f \rangle$, which is usually based on truncated Taylor expansions with respect to the normal coordinates about one equilibrium geometry. In the Franck-Condon approximation the transition dipole is assumed to remain constant during the electronic transition. While this approximation gives satisfactory results for strongly allowed transitions, it gives poor results for weakly-allowed or dipole-forbidden transitions. In this case, it is better to use the Franck-Condon Herzberg-Teller (FCHT) approximation, which also takes into account a linear variation of the electric dipole moment with respect to the normal coordinates **Q**:

$$\mu_{if}^{e} \approx \mu_{if}^{e}(\boldsymbol{Q}_{eq}) + \sum_{k=1}^{N} \frac{\partial \mu_{if}^{e}}{\partial Q_k} Q_k \qquad (2)$$

Finally, calculation of the overlap integrals requires a relation between the normal coordinates of initial- ($\overline{\mathbf{Q}}$) and final- ($\overline{\overline{\mathbf{Q}}}$) state, i.e. the basis sets used to expand the respective PES. The linear transformation proposed by Duschinsky is generally used for this purpose,[58]

$$\overline{\mathbf{Q}} = \mathbf{J}\overline{\overline{\mathbf{Q}}} + \mathbf{K} \qquad (3)$$

J represents the rotation matrix of the normal coordinates of the initial state during the transition and **K** is the shift vector due to the change in geometry. In addition to their role in the calculations, their representation gives an insight on the mode mixing upon the electronic transition and on the shift of the PESs, respectively, and can help understanding the reliability of the simulated vibronic spectra. The definition of **J** and, especially, **K** depends on the model used for the description of the transition.[52]

Equation (1) involves, in principle, infinite sums, and must be truncated in actual computations. Our implementation is based on a class-based prescreening to select *a priori* the most intense transitions.[44,59] Moreover, the computation of vibronic transitions is intrinsically parallel so that efficient implementations can make this step very fast (a few minutes in most cases). The bottleneck is by far the generation of the data needed to simulate the vibronic spectra, and in particular the computation of the Hessian matrices. In all models, the initial-state geometry must be optimized and the harmonic frequencies calculated. Then, the procedure to be followed for the final state varies. For AH, a geometry optimization is needed, followed by frequency calculation, while for VH, only the latter step must be done. In the approximated models, the force constants of the final state are not used, which is particular appealing since they are generally computed by numerical differentiation of TD-DFT energy gradients, which is the most time-consuming step of the whole procedure. For AS, there is still an optimization step while for VG, only the energy gradient is required. As a result, this latter model is particularly interesting for large systems, such as coumarin molecules encapsulated in inorganic matrices.[43] However, the approximations introduced can be excessive and lead to erroneous interpretations.

It should be noted that further refinement is possible by using more accurate vibrational energies for the two electronic states, either by applying simple scaling factors[60] or by computing the anharmonic frequencies[59,61]. The latter, which permits a systematic improvement of all frequencies, is particularly interesting when an analysis of the fine vibronic structure is sought but represents a steep increase of the overall computational cost. In the present case, the relatively low resolution of the experimental spectra means that broadening functions with large widths must be applied and so the anharmonic correction would be mostly hidden. Moreover, the effects of such a refinement on approximated models can be complex to interpret, as possible error compensations can impede the proper evaluation of the reliability of each model. As a result, frequencies were only computed at the harmonic level.

2.3 Computational details.

All DFT and/or TDDFT calculations have been performed with a locally modified version of the Gaussian09 suite of quantum chemical programs.[54]

As a first step, several hybrid and range-separated functionals, namely B3LYP,[15] PBE0,[14] M06,[38] M06-2X,[62] CAM-B3LYP,[29] LC-PBE,[63] ωB97X[64] and ωB97XD[36] have been used to compute the ground- and excited-state minima and Hessians necessary to generate the vibronic absorption spectra (within the Adiabatic Hessian / Franck-Condon approximations) of C307, C450, C460 and C480 reported in **Figure 1**. M06-HF[38] has been also considered but it systematically gave incorrect excited-state geometries for the systems of interest (breaking of planar symmetry), which resulted in too large shift vector and mode mixing, a poor spectrum convergence and a significantly different band-shape. Optimally tuned, range-separated functionals such as LC-PBE* and LC-PBE0* have not been considered here. Indeed, while they have been shown to improve the vibronic band shapes obtained with the non-tuned LC-PBE approach, they do not statistically yield more accurate spectra than standard hybrid functionals.[65]

In all calculations we have employed the 6-311++G(d,p) basis set, which has been shown to provide converged vibronic couplings by Jacquemin *et al.*[47] whereas solvent effects have been accounted for by using the polarizable continuum model.[66]

After the assessment of the aforementioned functionals, we used the ωB97X functional to compare the one-photon absorption spectra computed with different models, while the effect of the Herzberg-Teller contributions was studied with the adiabatic Hessian model. A compact notation will be used in the following to designate both the model describing the transition (VG, VH, AS, AH) and the approximation of the electronic transition dipole moment (FC, FCHT), where the two sets of acronyms are combined (for instance, AH|FC). As explained above, those models require the same data for the initial state, namely the harmonic frequencies for the equilibrium structure, but differ for the final state. For adiabatic approaches, AS and AH, we performed a geometry optimization followed

by frequency calculations. The adiabatic shift approximation is then readily obtained by ignoring those frequencies, so that only the equilibrium geometry is considered. For the VG approach, the optimized geometry of the initial state is used in the final state as the reference structure at which energy gradients are computed. Since frequency calculations for the excited state are performed at the TDDFT level by numerical differentiation of analytical forces, this step has a high computational cost, which can quickly become unsustainable for large systems. Regarding the vibronic calculations themselves, the sum-over-states approach with an explicit treatment of the individual vibronic transitions and the class-based prescreening method described previously has been used, where the class refers to the number of simultaneously excited modes in the final state. In order to achieve a good spectrum convergence (at least 90%), the excitations belonging to the first class (overtones) were included up to 30 quanta, those belonging to the second class (2-state combinations) up to 20 quanta for each excited mode, and a maximum of 10^9 transitions were considered in each class up to the seventh. Lower convergences were obtained for AH and VG with C480 (87 and 81%, respectively). A known issue with VH, observed in this work as well, is the likely presence of imaginary frequencies, often related to the limitations of the harmonic representation of the PES. In our case, 2 imaginary frequencies were found for C307, C450 and C460, and 1 for C480. Several strategies can be adopted to overcome this problem in the vibronic calculations. Hazra and Nooijen[67] have proposed an anharmonic treatment of the modes with imaginary frequencies. To do so, the system is first divided in two blocks, one containing the modes to be treated anharmonically and the other one containing the rest of the modes treated at the harmonic level. However, the definition of the blocks can be far from straightforward when the couplings between the modes are strong. This was indeed a problem here, but, since the corresponding imaginary frequencies were low, thus providing a marginal contribution to the vibronic spectrum, the approach proposed by Ferrer and Santoro[68] was adopted, namely to multiply all imaginary frequencies by *-i*.

As mentioned above, geometry optimizations and frequency calculations of all the coumarin molecules in methylcyclohexane and acetonitrile were performed employing the integral equation

formalism for the polarizable continuum model (IEF-PCM,[69] referred to simply as PCM in the following).

At variance with the simple case of electronic absorption spectra calculations where the non-equilibrium solute-solvent regime is usually employed,[70] the definition of the physically consistent solvation regime to be used in vibronic calculations must be done with care since both electronic and vibrational solvent degrees of freedom can follow the solute charge density evolving in time.[71] Depending on the time scale of such evolution, it might be assumed that some of the solvent's nuclear degrees of freedom remain static while others can relax along with the solute. Since we are not studying time-dependent spectra but stationary ones, which means that the molecule has the time to relax to the excited-state minimum and both the fast and slow solvent degrees of freedom are in equilibrium with the solute, we have employed the equilibrium solvation regime. This model is more consistent with the adiabatic treatment of the excited-state PES.[72] The vertical models in this case must be considered approximations of the adiabatic ones and thus the equilibrium solvation regime has been applied to them too.

The default parameters of Gaussian 09 Rev. D.01 were used for the construction of the cavity, built as the union of interlocked spheres centered on each atom of the solute with the following radii (in Å): 1.443 for hydrogen, 1.925 for carbon, 1.830 for nitrogen and 1.750 for oxygen, each multiplied by a factor of 1.1. The static and optical dielectric constants used for the solvents are 2.024 and 2.025, respectively for methylcyclohexane and 35.68 and 1.8069 for acetonitrile.

Since the experimental spectra were recorded at room temperature, vibronic calculations have to take into account the likely presence of hot bands. Temperature effects were simulated with the protocol described in ref.[56]. Using a temperature of 298.15 K, all initial vibrational states with at most 3 simultaneously excited modes and a Boltzmann population greater or equal to 25% of the vibrational ground state's were included in the summation given in eq. 1.

The stick spectra at room temperature were then smoothed with Gaussian distribution functions in order to reproduce the inhomogeneous broadening present from the experimental conditions. The half-width at half-maximum (HWHM) values used in the simulated spectra were chosen to match as closely as possible the experimental counterparts.

Results and Discussions

3.1 Vibrationally resolved absorption spectra: comparison between experiment and theory.

The absorption spectra of C307, C450, C460 and C480 recorded in methylcyclohexane and acetonitrile are reported in **Figure 2**. The overall spectra of the four coumarins are quite similar with a first band at around 340-380 nm due to the first dipole-allowed $\pi \rightarrow \pi^*$ transition from the highest occupied molecular orbital (HOMO) to the lowest unoccupied molecular orbital (LUMO), shown in **Figure S1** of the Supporting Information**.** As already noted for other 7-aminocoumarin derivatives,[41,43,73] the $S_1 \leftarrow S_0$ transition has a partial intra-molecular charge transfer character from the N-alkyl groups to the carbonyl. In fact, the HOMO is delocalized on the whole molecule, with significant contribution from the π orbitals of the "central" benzenic ring and the orbitals localized on the N,N-dialkyl group whereas the LUMO is mainly localized on the "quinone-like" terminal ring with a significant contribution of the π^* orbital of the carbonyl groups.[41,73]

The vibrational structure of the first band is clearly observed when the spectra are recorded in methylcyclohexane, whereas it is lost in acetonitrile whose higher polarity also leads to a red shift of the spectra by about 20 nm. Therefore, we will focus on methylcyclohexane in the following to assess the performance of functionals belonging to different families, while discussion on acetonitrile will be limited to the analysis of the normal modes.

The first band of C307 is composed of three peaks at about 385, 367 and 352 nm with the second peak more intense than the others and a shoulder around 325 nm. A similar shape is observed for the

first band of C450 even though four peaks are now recognizable (at about 360, 353, 344 and 330 nm) together with a more pronounced shoulder around 305 nm. The first band of C460 and C480 presents quite a different shape, showing three peaks at about 369, 361 and 351 nm for C460 and only two peaks (at 378 and 362 nm) for C480, all with comparable intensities (actually the peaks at 351 (C460) and 362 (C480) nm are slightly more intense).

The computation of the vibronic transitions represents a very demanding test for electronic structure methods. First, it makes possible the reproduction of the asymmetry of the band-shape, leading to a more correct definition of the absorption maximum. Second, it requires a proper calculation of the vibrational frequencies in addition to the electronic transition energy. In order to select the most suitable functional, the most refined vibronic models, namely AH and VH, should be preferred and, among them, we chose AH, which treats both electronic states at the same level, whereas VH could introduce some error compensation or numerical noise from the extrapolation of the excited state energy minimum, in addition to suffering directly from the PES anharmonicity. Since the transitions are strongly allowed, the Franck-Condon approximation was employed. The calculations have been carried out taking into account temperature effects within the TI formalism as described in the previous section. The vibronic spectra of the four investigated 7-aminocoumarin molecules in methylcyclohexane computed at the AH|FC level with 8 functionals are plotted in **Figure 3**. In order to compare the electronic structure methods, a single broadening method (with half-widths at half-maximum of 405 cm^{-1}) was used for all, chosen to facilitate the comparison with experiment.

The wavelengths corresponding to the vertical excitation energies and the central vibronic peaks computed with different functionals are reported in Table 1 and compared with the experimental data corresponding to the central and more intense peak.

Figure 3 shows that the PBE0 and M06 global-hybrid functionals yield vibronic transition energies in the closest agreement with experiment (within +2, -7, -4 and +2 nm for C307, C450, C460 and C480, respectively). B3LYP leads to vibronic transitions red-shifted by about 20 nm with respect to

experiment, while all the other functionals show larger discrepancies, with blue-shifts up to 50-60 nm, as in the case of LC-PBE. While PBE0 and M06 provide the best transition energies, they are not satisfactory for the band shape since the relative intensities of the vibronic transitions are not well reproduced for all the molecules investigated. In fact, the first peak is always more intense than the second one. Agreement with experiment is better with CAM-B3LYP and wB97XD, which have similar band-shapes, which is further improved in the case of M06-2X. The best overall shapes are provided by the LC-PBE and ωB97X functionals, for which the second (central) peak is more intense than the others (first and third) for all the coumarin molecules. However, closer examination of the spectra reveals that the ωB97X functional performs slightly better than LC-PBE, as shown in **Figure 4**. In this figure a broadening of 540 cm^{-1} was used in order to compare better the theoretical and experimental band-shapes. Moreover, to ease comparison, the computed spectra have been shifted to match the experimental absorption maxima. In fact, ωB97X yields better optical shapes than LC-PBE for C450, C460 and C480 (in particular for the lower energy components of the band) while only for C307 the opposite is true.

In **Figure 5** are reported the vibronic spectra of C480 at both T = 0K and T = 300K with broadening used to match the experiment. As previously mentioned, temperature effects cannot be simply reproduced by using inhomogeneous broadening functions with larger half-widths at half-maximum, as the relative intensities of the peaks show that the first band is accurately reproduced by the room temperature calculations but not at null temperature (only transitions from the vibrational ground state). Moreover, the third band appears to have a distinct maximum in 0K calculations, whereas the experimental and room-temperature simulation both show only a shoulder.

As shown in the ESI, the poorer agreement with the experimental spectrum of C307 regarding the lower-energy wing can be related to less accurate geometries computed at the ωB97X level compared to LCPBE, while the harmonic frequencies are properly reproduced. Since this effect can be assumed

to be consistent with the different vibronic models studied in the following, ωB97X can be satisfactorily used for this molecule as well.

In a recent benchmark on anthraquinone derivatives, Jacquemin *et al*.[47] found that global hybrids like B3LYP and PBE0 provide very good wavelengths but incorrect relative intensities; global hybrids with a larger amount of HF exchange like M06-2X blue-shift the peak positions, but give correct band-shapes, whereas long-range corrected functionals like CAM-B3LYP and ωB97XD gave satisfactorily results. Some of us[74] performed a similar investigation on two coumarin molecules finding that the CAM-B3LYP and M06-2X functionals provide the best intensity patterns. As shown here, a correct reproduction of the spectral band-shape requires a proper account of the vibronic structure. In this context, it is evident that a simple comparison of the computed vertical energies with the experimental λ_{max} is not sufficient to assess the accuracy and validate the choice of the functional, and that a correct definition of the computational protocol requires an extensive study of the vibronic structure as well. Moreover, it is also evident that, although no single functional provides simultaneously highly accurate positions and intensities of the different vibronic transitions, in all cases LC-PBE and particularly ωB97X represent the best compromises.

Another fast and efficient alternative to reproduce accurately the vibronic spectra could be to shift the spectrum obtained with a functional that provides a good band-shape (ωB97X and LC-PBE in this case) by a factor ($\Delta\lambda$) given by the difference in VEEs computed with PBE0 and with the chosen functional ($\Delta\lambda = \lambda_{VE,PBE0} - \lambda_{VE,XCF}$, where XCF is the functional used to compute the spectrum).

The vibronic spectra of C307, C450, C460 and C480 computed (in methylcyclohexane) by combining the ωB97X vibronic shape with the PBE0 VEEs shifts (denoted ωB97X/PBE0 hereafter) are compared with the experimental ones in **Figure 6.** Both broadened and stick spectra were shifted by $\Delta\lambda$ values of +47, +36, +41 and +47 for C307, C450, C460 and C480, respectively. The figure shows that by adopting this approach, both the shapes and positions of the vibronic spectra can be well reproduced. In fact, the differences between the positions of the experimental and theoretical spectra

are always within 10 nm. As a matter of fact, a constant shift within a class of related molecules (about 40 nm in the present case) is usually sufficient.

Effects of the excited state PES approximations on the vibronic spectra.

The definition of the most reliable electronic structure method paves the way to the study of different vibronic models, namely adiabatic Hessian and shift, and vertical Hessian and gradient. As mentioned above, AS and VG have the advantage of being more affordable since they do not require the calculation of the excited-state frequencies, thus being better adapted to studies over an extensive sample of different systems. The vibronic spectra obtained with the AH, AS, VH and VG models and the FC approximation are reported in **Figures 7** and **8**. Two different broadenings were used. The lower-resolution spectra, in **Figure 7**, match the experimental data available in this study.

In general, AH, VH and AS have similar band-shapes and for the 4 compounds, 3 summits are visible, together with a shoulder in the left-most tail of the band-shape. At variance, the VG spectra are on overall less distinctive and for C307, C450, and to a lower extent C480. For C450, the 3 summits are merged with the 2 outermost ones appearing as prominent shoulders, while for C307, the leftmost peak has a relative height lower than with the other models. The only exception is C460 where the band-shape is very similar to the other ones. For this system, all 4 models give about the same result. This hints at a high similarity between the initial- and final-state PESs. A final remark regards C450 where the AH|FC band is very wide. The lack of such a feature with the approximated model AS|FC implies that a strong mode mixing is present. The fact that VH|FC does not exhibit this large tail in the blue region can be indicative of limitations in the underlying Cartesian coordinate description on which the normal coordinates have been built.

In order to provide a more detailed comparison between the spectra, the relative intensities of the second (most intense) band with respect to the first band, which contains the “0-0” transitions, computed with different adiabatic and vertical models are reported in Table 2, together with the

experimental one. The table shows that for C307, the intensity ratio between the second and first band is better reproduced by the VG|FC scheme. As it will be shown later this is caused by an error compensation due to the absence of mode mixing. However, is has to be pointed out that in the other cases, AH|FC yields the better agreement with the experimental data, while VG|FC yields poorer results.

By increasing the resolution (i.e. by lowering the widths of the distribution functions applied to the vibronic transitions to simulate the experimental broadening) additional features can be observed. The higher resolution spectra are shown in **Figure 8**. In line with the observation made for **Figure 7**, the VG|FC spectra remain mostly featureless even with this low HWHM. However, it is now possible to isolate the 3 summits, which could already be brought out with the 3 models at the lower resolution. As before, C460 is an exception and the fine structure is observable with VG as well. It is noteworthy that, contrary to expectations, the AH|FC spectra show rather broad bands with many shoulders. A richer structure, with more peaks is visible with AS|FC, thus confirming the significant mode mixing. In addition to being a potential issue in the analysis of high resolution spectra, a strong mode mixing often results in non-negligible contributions from many transitions, preventing a precise band assignment. Indeed, comparison of the VH and AH stick spectra shown in **Figure 9** shows that the AH|FC band-shape is formed by a multitude of transitions of low-to-medium intensities, with few distinguishable peaks. At variance, the VH|FC stick spectra exhibit a more contrasted structure and specific lines can be isolated and analyzed to propose a band-assignment. C480 represents an exception where neither spectrum is easily interpretable due to an extremely rich peak structure. The difference is more marked in the spectra where the temperature effects have been ignored (T=0K), reported in **Figure 10**.

As a concluding remark, it is interesting to note the shifted position of the band-shape maxima between the different models, shown in **Figure 7**. Indeed, the vibronic structure depends on the position of the transition between the vibrational ground states of the initial and final electronic states,

i.e. the 0-0 transition. The associated energy corresponds to the energy difference between the minima of the PES, including the zero-point vibrational energies. In this respect, AH provides the most correct definition, while in VH, the excited-state PES minimum is extrapolated by assuming that the PES is parabolic and the frequencies are computed outside the minimum. AS and VG introduce the further approximation that the vibrational frequencies (hence the zero point energies) of the two electronic states are equal. The combination of various approximations may lead to error compensation or enhancement with respect to experiment. The AH|FC and VH|FC spectra are compared to their experimental counterpart in **Figure 11**. For all systems, the VH|FC band-shape is farther from the experimental spectrum than AH|FC, which further justifies the choice of the latter as the reference method to select the most suitable density functional. Adding the Herzberg-Teller contributions to the calculations leads to slight changes to the band-shapes in all cases. More specifically, the lower-energy summit has a slightly higher intensity with respect to the central, predominant one, while the higher energy one is toned down and appears in some cases as a prominent shoulder. Those changes are consistent with the observed band-shapes, except for C450 where the remarkable agreement in the relative intensities of the 2 lower-energy peaks is slightly worsened. Nevertheless, the overall impact on the band-shape and in particular the position of its maximum is negligible. It should be noted that the FCHT approximation requires the gradient of the electronic transition dipole moment, currently obtained by numerical differentiation along the Cartesian coordinates in the same way as the excited-state frequencies. For this reason, inclusion of those contributions spoils the computational advantages of approximated models, like AS and VG.

Analysis of the vibronic spectra of C307 and C460 molecules.

Figure 12 compares the experimental and theoretical vibronic spectra of C307 and C460 in methylcyclohexane and acetonitrile solvents. The stick spectra with the main vibronic contributions are also reported, and together with the broadened spectra, have been shifted so that the most intense peak in methylcyclohexane coincides with its experimental counterpart. Comparing **Figures 9** and

10, the trend between the stick spectra with or without temperature effects is similar. As the most intense transitions arise from the ground state, the present analysis will be limited to the latter, using the spectra simulated at T=0K for the sake of readability.

Analogous data for the other coumarin molecules are reported in **Figure S2** of the Supporting Information and will not be described here since the vibronic contributions are similar.

The agreement between the experimental and theoretical spectra of C307 in methylcyclohexane is excellent, also concerning the separation between the three main peaks. As expected, the first peak of C307 is associated to the 0-0 transition whereas the other two peaks are composed of a blend of several vibrational modes. However, the most intense vibronic transitions can be ascribed to single quanta excitations of modes 16 (296 cm^{-1} with respect to the 0-0 line), 21 (409 cm^{-1}), 37 (818 cm^{-1}), 72 (1591 cm^{-1}), 74 (1695 cm^{-1}) and 75 (1759 cm^{-1}) of the excited state, respectively.

A graphical representation of these modes can be found in **Figure S3** of the Supporting Information. Modes 16 and 21 correspond to the wagging of the methyl and ethyl groups and to the breathing of the aromatic benzopyrone ring. Modes 37, 72 and 74 correspond to the stretching of the same ring and to displacements of the hydrogen atoms, whereas mode 75 is related to the C=O stretching. Finally, the shoulder at about 350 nm is due to the simultaneous excitation of modes 72 and 74 (3286 cm^{-1} with respect to the 0-0 line) 72-75 (3350 cm^{-1}) and 74-75 (3454 cm^{-1}).

The first peak of C460 is again associated to the 0-0 transition, whereas the more intense vibronic transitions can be ascribed to single quanta excitations of modes 22 (496 cm^{-1} with respect to the 0-0 line), 23 (517 cm^{-1}), 28 (668 cm^{-1}), 51 (1211 cm^{-1}), 65 (1445 cm^{-1}), 77 (1579 cm^{-1}), 78 (1687 cm^{-1}) and 79 (1739 cm^{-1}) of the excited state, respectively.

A graphical representation of these modes can be found in **Figure S3** of the Supporting Information. Modes 22, 23 and 28 correspond to the wagging of the methyl and ethyl groups and to the breathing of the aromatic benzopyrone ring. Modes 51, 65, 77 and 78 correspond to displacements of the

aromatic hydrogens and stretching of the C-C bond in the same ring while mode 79 is related to the C=O stretching. The shoulder near 335 nm is due to the simultaneous excitation of modes 77, 78 and 79.

The vibronic spectra of C307 and C460 in acetonitrile (**Figure 11**, bottom panels) are blue-shifted by about 20 nm with respect to those in methylcyclohexane, in good agreement with the experimental data. In order to reproduce well the band shape, the stick spectra were broadened by a larger Gaussian functions with HWHM of 810 cm^{-1}. With this empirical broadening, the vibronic structure is lost and the experimental band-shape is recovered. The employment of larger HWHM in polar solvents with respect to apolar ones is justified by the Marcus's relationship connecting the inhomogeneous broadening with the solvent re-organization energy which is bigger for polar solvents.[75,76]

The stick spectra are similar to those computed in methyl-cyclohexane, but spread over a larger spectral interval, and new combined transitions appear. In fact, the peaks of the C307 molecule associated to the simultaneous excitation of modes 20-16, 75-16 and 75-20 found respectively at 707, 2029 and 2141 cm^{-1} from the 0-0 transitions show stronger intensities and this is also the case for the peak at 3463 cm^{-1} from the 0-0 transition associated to the double excitation of mode 75.

In the case of C460, the change in solvent polarity leads to more intense peaks for the transitions associated to the single excitation of mode 79, to the simultaneous excitation of modes 79-23 (2244 cm^{-1}) and to the double excitation of mode 79 (3451 cm^{-1}).

Conclusions.

We have assessed the performance of several global and range-separated hybrid functionals in reproducing the vibrationally-resolved absorption spectra of four 7-aminocoumarin molecules of technological interest collected in different solvents. In agreement with previous investigations, we have found that the specific DFT functional used to calculate vibronic spectra has a significant impact on the results. In particular, the major discrepancies are observed in the computation of the absolute

positions of the simulated vibrationally resolved electronic spectra, with PBE0 and M06 functionals providing the best positions. At variance, ωB97X and LC-PBE provide the most accurate band-shape. As a consequence, combination of vibronic couplings computed by using the ωB97X functional with PBE0 vertical energies gives the possibility to obtain good band shapes and positions with differences between experimental and theoretical band maxima lower than 10 nm.

Comparison between AH and VH models has shown that they provide similar results as long as highly detailed band-shapes are not required. The higher mode mixing in AH results in visible contributions from a huge number of transitions, hence in an attenuation of the features of the band-shape. At variance, VH provides a sharper band-shape but it overestimates the energy of the absorption maximum. The cheapest model (VG) is not able to reproduce the experimental band-shape even at low resolution, except for C460. The slightly more expensive AS model performs much better, and should be preferred whenever reduction of the computational cost becomes critical.

Detailed analysis of the vibronic contributions to the spectra of the investigated molecules revealed that the most intense vibronic transitions can be ascribed to single quanta excitations, whereas the shoulder at lower wavelengths is due to the combinations of the simultaneous excitation of high frequency modes and double excitations of single modes.

Acknowledgements

This work was supported by the Italian Ministero dell'Istruzione, dell' Università e della Ricerca (MIUR) through the Programma di ricerca di rilevante interesse nazionale" (PRIN) Grant 2010C4R8M8_002 entitled “Nanoscale functional Organization of (bio)Molecules and Hybrids for targeted Application in Sensing, Medicine and Biotechnology" and the ``Futuro in Ricerca" (FIRB) Grants RBFR1248UI 002 entitled “Novel Multiscale Theorethical/Computational Strategies for the Design of Photo and Thermo responsive Hybrid Organic-Inorganic Components for Nanoelectronic

Circuits" and RBFR122HFZ entitled “Progettazione di materiali nanoeterogenei per la conversione di energia solare”.

Supporting Information Available

The Kohn-Sham HOMO and LUMO orbitals of the investigated molecule, the ωB97X and experimental vibronic spectra of C450 and C480 molecules in methylcyclohexane and acetonitrile solvents and a representation of the more important normal models of the investigated molecules are reported in the supporting information. This material is available free of charge via the internet at the http://pubs.acs.org/.

References

(1) Cohen, A. J.; Mori-Sánchez, P.; Yang, W. Challenges for Density Functional Theory. *Chem. Rev.* **2012**, *112*, 289–320.

(2) Dreuw, A.; Head-Gordon, M. Single-Reference Ab Initio Methods for the Calculation of Excited States of Large Molecules. *Chem. Rev.* **2005**, *105*, 4009–4037.

(3) Runge, E.; Gross, E. K. U. Density-Functional Theory for Time-Dependent Systems. *Phys. Rev. Lett.* **1984**, *52*, 997–1000.

(4) Cimino, P.; Pedone, A.; Stendardo, E.; Barone, V. Interplay of Stereo-Electronic, Environmental, and Dynamical Effects in Determining the EPR Parameters of Aromatic Spin-Probes: INDCO as a Test Case. *Phys. Chem. Chem. Phys.* **2010**, *12*, 3741–3746.

(5) Pedone, A.; Biczysko, M.; Barone, V. Environmental Effects in Computational Spectroscopy: Accuracy and Interpretation. *Chemphyschem* **2010**, *11*, 1812–1832.

(6) Pedone, A.; Prampolini, G.; Monti, S.; Barone, V. Absorption and Emission Spectra of Fluorescent Silica Nanoparticles from TD-DFT/MM/PCM Calculations. *Phys. Chem. Chem. Phys.* **2011**, *13*, 16689.

(7) Pedone, A.; Prampolini, G.; Monti, S.; Barone, V. Realistic Modeling of Fluorescent Dye-Doped Silica Nanoparticles: A Step Toward the Understanding of Their Enhanced Photophysical Properties. *Chem. Mater.* **2011**, *23*, 5016–5023.

(8) Adamo, C.; Jacquemin, D. The Calculations of Excited-State Properties with Time-Dependent Density Functional Theory. *Chem. Soc. Rev.* **2013**, *42*, 845.

(9) Mennucci, B. Modeling Environment Effects on Spectroscopies through QM/classical Models. *Phys. Chem. Chem. Phys.* **2013**, *15*, 6583–6594.

(10) Jacquemin, D.; Mennucci, B.; Adamo, C. Excited-State Calculations with TD-DFT: From Benchmarks to Simulations in Complex Environments. *Phys. Chem. Chem. Phys.* **2011**, *13*, 16987–16998.

(11) Presti, D.; Labat, F.; Pedone, A.; Frisch, M. J.; Hratchian, H. P.; Ciofini, I.; Menziani, M. C.; Adamo, C. Computational Protocol for Modeling Thermochromic Molecular Crystals: Salicylidene Aniline As a Case Study. *J. Chem. Theory Comput.* **2014**, *10*, 5577–5585.

(12) Jacquemin, D.; Perpete, E. A.; Assfeld, X.; Scalmani, G.; Frisch, M. J.; Adamo, C. The Geometries, Absorption and Fluorescence Wavelengths of Solvated Fluorescent Coumarins: A CIS and TD-DFT Comparative. *Chem. Phys. Lett.* **2007**, *438*, 208–212.

(13) Jacquemin, D.; Wathelet, V.; Perpete, E. A.; Adamo, C. Extensive TD-DFT Benchmark: Singlet-Excited States of Organic Molecules. *J. Chem. Theory Comput.* **2009**, *5*, 2420–2435.

(14) Adamo, C.; Barone, V. Toward Reliable Density Functional Methods without Adjustable Parameters: The PBE0 Model. *J. Chem. Phys.* **1999**, *110*, 6158–6170.

(15) Becke, A. D. Density-Functional Thermochemistry. III. The Role of Exact Exchange. *J. Chem. Phys.* **1993**, *98*, 5648.

(16) Champagne, B.; Perpète, E. A.; Gisbergen, S. J. A. van; Baerends, E.-J.; Snijders, J. G.; Soubra-Ghaoui, C.; Robins, K. A.; Kirtman, B. Assessment of Conventional Density Functional Schemes for Computing the Polarizabilities and Hyperpolarizabilities of Conjugated Oligomers: An Ab Initio Investigation of Polyacetylene Chains. *J. Chem. Phys.* **1998**, *109*, 10489–10498.

(17) Dreuw, A.; Head-Gordon, M. Failure of Time-Dependent Density Functional Theory for Long-Range Charge-Transfer Excited States: The Zincbacteriochlorin-Bacterlochlorin and Bacteriochlorophyll-Spheroidene Complexes. *J. Am. Chem. Soc.* **2004**, *126*, 4007–4016.

(18) Tozer, D. J. Relationship between Long-Range Charge-Transfer Excitation Energy Error and Integer Discontinuity in Kohn-Sham Theory. *J. Chem. Phys.* **2003**, *119*, 12697–12699.

(19) Presti, D.; Pedone, A.; Menziani, M. C.; Civalleri, B.; Maschio, L. Oxalyl Dihydrazide Polymorphism: A Periodic Dispersion-Corrected DFT and MP2 Investigation. *Crystengcomm* **2014**, *16*, 102–109.

(20) Pedone, A.; Presti, D.; Menziani, M. C. On the Ability of Periodic Dispersion-Corrected DFT Calculations to Predict Molecular Crystal Polymorphism in Para-Diiodobenzene. *Chem. Phys. Lett.* **2012**, *541*, 12–15.

(21) Presti, D.; Pedone, A.; Menziani, M. C. Unraveling the Polymorphism of [(p-cymene)Ru(κN-INA)Cl2] through Dispersion-Corrected DFT and NMR GIPAW Calculations. *Inorg. Chem.* **2014**, *53*, 7926–7935.

(22) Jacquemin, D.; Femenias, A.; Chermette, H.; Ciofini, I.; Adamo, C.; Andre, J. M.; Perpete, E. A. Assessment of Several Hybrid DFT Functionals for the Evaluation of Bond Length Alternation of Increasingly Long Oligomers. *J. Phys. Chem. A* **2006**, *110*, 5952–5959.

(23) Peach, M. J. G.; Benfield, P.; Helgaker, T.; Tozer, D. J. Excitation Energies in Density Functional Theory: An Evaluation and a Diagnostic Test. *J. Chem. Phys.* **2008**, *128*, 044118.

(24) Heyd, J.; Scuseria, G. E.; Ernzerhof, M. Hybrid Functionals Based on a Screened Coulomb Potential. *J. Chem. Phys.* **2003**, *118*, 8207–8215.

(25) Peach, M. J. G.; Helgaker, T.; Salek, P.; Keal, T. W.; Lutnaes, O. B.; Tozer, D. J.; Handy, N. C. Assessment of a Coulomb-Attenuated Exchange-Correlation Energy Functional. *Phys. Chem. Chem. Phys.* **2006**, *8*, 558–562.

(26) Toulouse, J.; Colonna, F.; Savin, A. Long-Range-Short-Range Separation of the Electron-Electron Interaction in Density-Functional Theory. *Phys. Rev. A* **2004**, *70*, 062505.

(27) Tawada, Y.; Tsuneda, T.; Yanagisawa, S.; Yanai, T.; Hirao, K. A Long-Range Corrected Time-Dependent Density Functional Theory. *J. Chem. Phys.* 2004, *120*, 8425–8433.

(28) Yanai, T.; Harrison, R. J.; Handy, N. C. Multiresolution Quantum Chemistry in Multiwavelet Bases: Time-Dependent Density Functional Theory with Asymptotically Corrected Potentials in Local Density and Generalized Gradient Approximations. *Mol. Phys.* **2005**, *103*, 413–424.

(29) Yanai, T.; Tew, D. P.; Handy, N. C. A New Hybrid Exchange-Correlation Functional Using the Coulomb-Attenuating Method (CAM-B3LYP). *Chem. Phys. Lett.* **2004**, *393*, 51–57.

(30) Baer, R.; Neuhauser, D. Density Functional Theory with Correct Long-Range Asymptotic Behavior. *Phys. Rev. Lett.* **2005**, *94*, 043002.

(31) Grimme, S.; Neese, F. Double-Hybrid Density Functional Theory for Excited Electronic States of Molecules. *J. Chem. Phys.* **2007**, *127*, 154116.

(32) Muniz-Miranda, F.; Menziani, M. C.; Pedone, A. Assessment of Exchange-Correlation Functionals in Reproducing the Structure and Optical Gap of Organic-Protected Gold Nanoclusters. *J. Phys. Chem. C* **2014**, *118*, 7532–7544.

(33) Muniz-Miranda, F.; Menziani, M. C.; Pedone, A. On the Opto-Electronic Properties of Phosphine and Thiolate-Protected Undecagold Nanoclusters. *Phys. Chem. Chem. Phys.* **2014**, *16*, 18749.

(34) Muniz-Miranda, F.; Menziani, M. C.; Pedone, A. DFT and TD-DFT Assessment of the Structural and Optoelectronic Properties of an Organic–Ag14 Nanocluster. *J. Phys. Chem. A* **2015**, *119*, *5088-5098*.

(35) Ernzerhof, M.; Scuseria, G. E. Assessment of the Perdew-Burke-Ernzerhof Exchange-Correlation Functional. *J. Chem. Phys.* **1999**, *110*, 5029–5036.

(36) Chai, J.-D.; Head-Gordon, M. Long-Range Corrected Hybrid Density Functionals with Damped Atom-Atom Dispersion Corrections. *Phys. Chem. Chem. Phys.* **2008**, *10*, 6615–6620.

(37) Zhao, Y.; Schultz, N. E.; Truhlar, D. G. Design of Density Functionals by Combining the Method of Constraint Satisfaction with Parametrization for Thermochemistry, Thermochemical Kinetics, and Noncovalent Interactions. *J. Chem. Theory Comput.* **2006**, *2*, 364–382.

(38) Zhao, Y.; Truhlar, D. G. The M06 Suite of Density Functionals for Main Group Thermochemistry, Thermochemical Kinetics, Noncovalent Interactions, Excited States, and Transition Elements: Two New Functionals and Systematic Testing of Four M06-Class Functionals and 12 Other Functionals. *Theor. Chem. Acc.* **2008**, *120*, 215–241.

(39) Zhao, Y.; Truhlar, D. G. Exploring the Limit of Accuracy of the Global Hybrid Meta Density Functional for Main-Group Thermochemistry, Kinetics, and Noncovalent Interactions. *J. Chem. Theory Comput.* **2008**, *4*, 1849–1868.

(40) Improta, R.; Barone, V. Interplay between "Neutral" and "Charge-Transfer" Excimers Rules the Excited State Decay in Adenine-Rich Polynucleotides. *Angew. Chem.-Int. Ed.* **2011**, *50*, 12016–12019.

(41) Pedone, A.; Gambuzzi, E.; Barone, V.; Bonacchi, S.; Genovese, D.; Rampazzo, E.; Prodi, L.; Montalti, M. Understanding the Photophysical Properties of Coumarin-Based Pluronic-Silica (PluS) Nanoparticles by Means of Time-Resolved Emission Spectroscopy and Accurate TDDFT/stochastic Calculations. *Phys. Chem. Chem. Phys.* **2013**, *15*, 12360–12372.

(42) Improta, R.; Barone, V.; Santoro, F. Ab Initio Calculations of Absorption Spectra of Large Molecules in Solution: Coumarin C153. *Angew. Chem.-Int. Ed.* **2007**, *46*, 405–408.

(43) Pedone, A.; Bloino, J.; Barone, V. Role of Host–Guest Interactions in Tuning the Optical Properties of Coumarin Derivatives Incorporated in MCM-41: A TD-DFT Investigation. *J. Phys. Chem. C* **2012**, *116*, 17807–17818.

(44) Santoro, F.; Improta, R.; Lami, A.; Bloino, J.; Barone, V. Effective Method to Compute Franck-Condon Integrals for Optical Spectra of Large Molecules in Solution. *J. Chem. Phys.* **2007**, *126*, 084509.

(45) Dierksen, M.; Grimme, S. The Vibronic Structure of Electronic Absorption Spectra of Large Molecules: A Time-Dependent Density Functional Study on the Influence of "Exact" Hartree-Fock Exchange. *J. Phys. Chem. A* **2004**, *108*, 10225–10237.

(46) Stendardo, E.; Avila Ferrer, F.; Santoro, F.; Improta, R. Vibrationally Resolved Absorption and Emission Spectra of Dithiophene in the Gas Phase and in Solution by First-Principle Quantum Mechanical Calculations. *J. Chem. Theory Comput.* **2012**, *8*, 4483–4493.

(47) Jacquemin, D.; Bremond, E.; Planchat, A.; Ciofini, I.; Adamo, C. TD-DFT Vibronic Couplings in Anthraquinones: From Basis Set and Functional Benchmarks to Applications for Industrial Dyes. *J. Chem. Theory Comput.* **2011**, *7*, 1882–1892.

(48) Sheats, J. R.; Barbara, P. F. Molecular Materials in Electronic and Optoelectronic Devices. *Acc. Chem. Res.* **1999**, *32*, 191–192.

(49) Yang, Y.; Zou, J.; Rong, H.; Qian, G. D.; Wang, Z. Y.; Wang, M. Q. Influence of Various Coumarin Dyes on the Laser Performance of Laser Dyes Co-Doped into ORMOSILs. *Appl. Phys. B* **2007**, *86*, 309–313.

(50) Kozlov, V. G.; Parthasarathy, G.; Burrows, P. E.; Forrest, S. R.; You, Y.; Thompson, M. E. Optically Pumped Blue Organic Semiconductor Lasers. *Appl. Phys. Lett.* **1998**, *72*, 144–146.

(51) Schulz-Ekloff, G.; Wohrle, D.; van Duffel, B.; Schoonheydt, R. A. Chromophores in Porous Silicas and Minerals: Preparation and Optical Properties. *Microporous Mesoporous Mater.* **2002**, *51*, 91–138.

(52) Biczysko, M.; Bloino, J.; Santoro, F.; Barone, V. Time Independent Approaches to Simulate Electronic Spectra Lineshapes: From Small Molecules to Macrosystems. In *Computational Strategies for Spectroscopy, from Small Molecules to Nano Systems*; Barone, Vincenzo: Wiley, Chichester, 2011; pp 361–443.

(53) Baiardi, A.; Bloino, J.; Barone, V. General Time Dependent Approach to Vibronic Spectroscopy Including Franck–Condon, Herzberg–Teller, and Duschinsky Effects. *J. Chem. Theory Comput.* **2013**, *9*, 4097–4115.

(54) Frisch, M. J.; Trucks, G. W.; Cheeseman, J. R.; Scalmani, G.; Caricato, M.; Hratchian, H. P.; Li, X.; Barone, V.; Bloino, J.; Zheng, G.; Vreven, T.; Montgomery, J. A.; Petersson, G. A.; Scuseria, G. E.; Schlegel, H. B.; Nakatsuji, H.; Izmaylov, A. F.; Martin, R. L.; Sonnenberg, J. L.; Peralta, J. E.; Heyd, J. J.; Brothers, E.; Ogliaro, F.; Bearpark, M.; Robb, M. A.; Mennucci, B.; Kudin, K. N.; Staroverov, V. N.; Kobayashi, R.; Normand, J.; Rendell, A.; Gomperts, R.;

Zakrzewski, V. G.; Hada, M.; Ehara, M.; Toyota, K.; Fukuda, R.; Hasegawa, J.; Ishida, M.; Nakajima, T.; Honda, Y.; Kitao, O.; Nakai, H. *Gaussian 09*.

(55) Barone, V.; Bloino, J.; Biczysko, M.; Santoro, F. Fully Integrated Approach to Compute Vibrationally Resolved Optical Spectra: From Small Molecules to Macrosystems. *J. Chem. Theory Comput.* **2009**, *5*, 540–554.

(56) Bloino, J.; Biczysko, M.; Santoro, F.; Barone, V. General Approach to Compute Vibrationally Resolved One-Photon Electronic Spectra. *J. Chem. Theory Comput.* **2010**, *6*, 1256–1274.

(57) Macak, P.; Luo, Y.; Ågren, H. Simulations of Vibronic Profiles in Two-Photon Absorption. *Chem. Phys. Lett.* **2000**, *330*, 447–456.

(58) Duschinsky, F. *Acta Physicochim. U. R. S. S.* **1937**, *7*, 551.

(59) Santoro, F.; Lami, A.; Improta, R.; Bloino, J.; Barone, V. Effective Method for the Computation of Optical Spectra of Large Molecules at Finite Temperature Including the Duschinsky and Herzberg–Teller Effect: The Qx Band of Porphyrin as a Case Study. *J. Chem. Phys.* **2008**, *128*, 224311.

(60) Champagne, B.; Liégeois, V.; Zutterman, F. Pigment Violet 19 – a Test Case to Define a Simple Method to Simulate the Vibronic Structure of Absorption Spectra of Organic Pigments and Dyes in Solution. *Photochem. Photobiol. Sci.* **2015**, *14*, 444–456.

(61) Biczysko, M.; Bloino, J.; Brancato, G.; Cacelli, I.; Cappelli, C.; Ferretti, A.; Lami, A.; Monti, S.; Pedone, A.; Prampolini, G.; Puzzarini, C.; Santoro, F.; Trani, F.; Villani, G. Integrated Computational Approaches for Spectroscopic Studies of Molecular Systems in the Gas Phase and in Solution: Pyrimidine as a Test Case. *Theor. Chem. Acc.* **2012**, *131*, 1–19.

(62) Zhao, Y.; Truhlar, D. G. Density Functional for Spectroscopy: No Long-Range Self-Interaction Error, Good Performance for Rydberg and Charge-Transfer States, and Better Performance on Average than B3LYP for Ground States. *J. Phys. Chem. A* **2006**, *110*, 13126–13130.

(63) Tawada, Y.; Tsuneda, T.; Yanagisawa, S.; Yanai, T.; Hirao, K. A Long-Range-Corrected Time-Dependent Density Functional Theory. *J. Chem. Phys.* **2004**, *120*, 8425–8433.

(64) Chai, J.-D.; Head-Gordon, M. Systematic Optimization of Long-Range Corrected Hybrid Density Functionals. *J. Chem. Phys.* **2008**, *128*, 084106.

(65) Moore, B.; Charaf-Eddin, A.; Planchat, A.; Adamo, C.; Autschbach, J.; Jacquemin, D. Electronic Band Shapes Calculated with Optimally Tuned Range-Separated Hybrid Functionals. *J. Chem. Theory Comput.* **2014**, *10*, 4599–4608.

(66) Tomasi, J.; Mennucci, B.; Cammi, R. Quantum Mechanical Continuum Solvation Models. *Chem. Rev.* **2005**, *105*, 2999–3093.

(67) Hazra, A.; Nooijen, M. Comparison of Various Franck–Condon and Vibronic Coupling Approaches for Simulating Electronic Spectra: The Case of the Lowest Photoelectron Band of Ethylene. *Phys. Chem. Chem. Phys.* **2005**, *7*, 1759–1771.

(68) Ferrer, F. J. A.; Santoro, F. Comparison of Vertical and Adiabatic Harmonic Approaches for the Calculation of the Vibrational Structure of Electronic Spectra. *Phys. Chem. Chem. Phys.* **2012**, *14*, 13549–13563.

(69) Cancès, E.; Mennucci, B.; Tomasi, J. A New Integral Equation Formalism for the Polarizable Continuum Model: Theoretical Background and Applications to Isotropic and Anisotropic Dielectrics. *J. Chem. Phys.* **1997**, *107*, 3032–3041.

(70) Fukuda, R.; Ehara, M.; Nakatsuji, H.; Cammi, R. Nonequilibrium Solvation for Vertical Photoemission and Photoabsorption Processes Using the Symmetry-Adapted Cluster–configuration Interaction Method in the Polarizable Continuum Model. *J. Chem. Phys.* **2011**, *134*, 104109.

(71) Mennucci, B.; Cappelli, C.; Guido, C. A.; Cammi, R.; Tomasi, J. Structures and Properties of Electronically Excited Chromophores in Solution from the Polarizable Continuum Model Coupled to the Time-Dependent Density Functional Theory. *J. Phys. Chem. A* **2009**, *113*, 3009–3020.

(72) Egidi, F.; Bloino, J.; Cappelli, C.; Barone, V. A Robust and Effective Time-Independent Route to the Calculation of Resonance Raman Spectra of Large Molecules in Condensed Phases with

the Inclusion of Duschinsky, Herzberg–Teller, Anharmonic, and Environmental Effects. *J. Chem. Theory Comput.* **2014**, *10*, 346–363.

(73) Pedone, A. Role of Solvent on Charge Transfer in 7-Aminocoumarin Dyes: New Hints from TD-CAM-B3LYP and State Specific PCM Calculations. *J. Chem. Theory Comput.* **2013**, *9*, 4087–4096.

(74) Barone, V.; Biczysko, M.; Bloino, J.; Carta, L.; Pedone, A. Environmental and Dynamical Effects on the Optical Properties of Molecular Systems by Time-Independent and Time-Dependent Approaches: Coumarin Derivatives as Test Cases. *Comput. Theor. Chem.* **2014**, *1037*, 35–48.

(75) Marcus, R. A. Relation between Charge Transfer Absorption and Fluorescence Spectra and the Inverted Region. *J. Phys. Chem.* **1989**, *93*, 3078–3086.

(76) Ferrer, F. J. A.; Improta, R.; Santoro, F.; Barone, V. Computing the Inhomogeneous Broadening of Electronic Transitions in Solution: A First-Principle Quantum Mechanical Approach. *Phys. Chem. Chem. Phys.* **2011**, *13*, 17007–17012.

Table 1. Wavelengths of the second peak in the vibronic spectra of the four coumarins with various functionals at the AH|FC level of theory. In parenthesis are reported the wavelength corresponding to the vertical excitation energies.

Method	**C307**	**C450**	**C460**	**C480**
ωB97x	330 (313)	302 (294)	312 (299)	321 (307)
B3LYP	390 (375)	350 (341)	348 (353)	374 (367)
CAM-B3LYP	344 (331)	320 (308)	323 (314)	335 (324)
LC-PBE	311 (295)	294 (280)	297 (283)	306 (291)
ωB97xD	340 (327)	318 (305)	321 (311)	331 (320)
PBE0	370 (360)	339 (330)	347 (340)	359 (354)
M06	369 (360)	341 (333)	348 (342)	362 (356)
M06-2X	340 (337)	320 (306)	324 (315)	335 (324)
experimental	*366*	*343*	*351*	*362*

Table 2. Relative intensity of the second most intense band with respect to the first "0-0" band obtained with different vibronic models. All calculations were performed at the ωB97x level of theory.

Method	C307	C450	C460	C480
AH|FC	1.13	1.33	1.11	1.10
AS|FC	1.13	1.32	0.99	1.10
VH|FC	1.13	1.34	1.12	1.11
VG|FC	1.26	1.56	1.13	1.12
experimental	*1.30*	*1.31*	*1.09*	*1.09*

Figures.

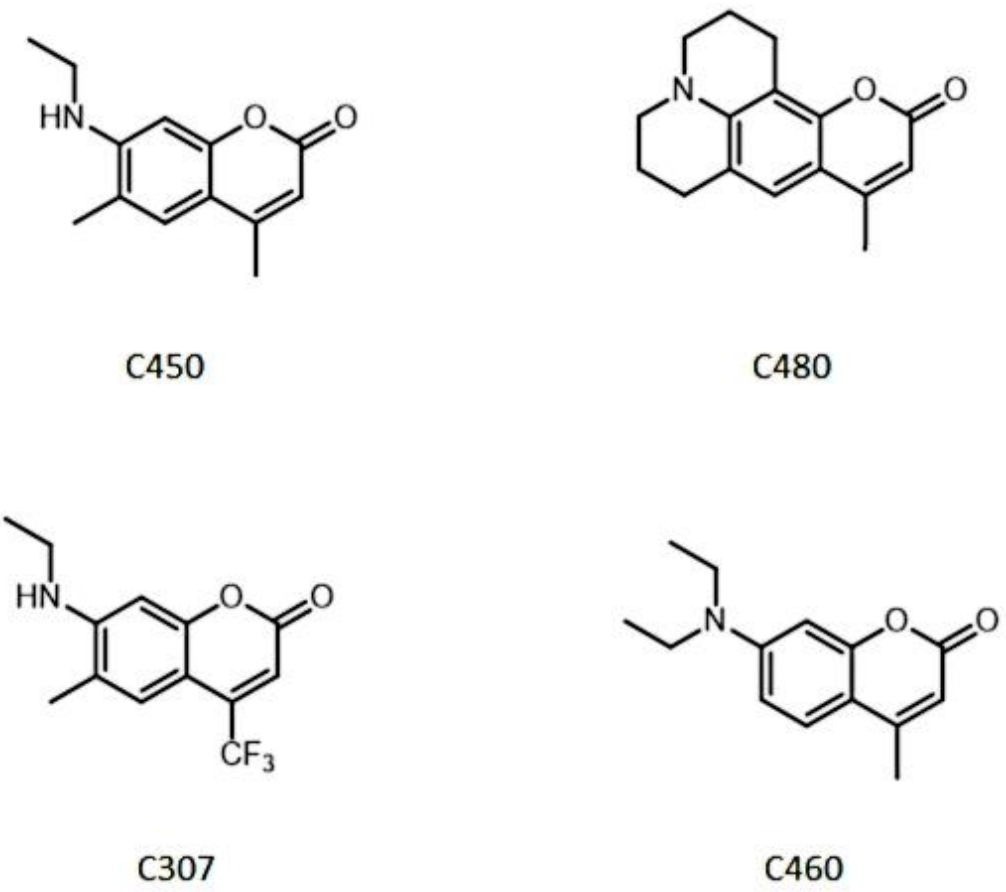

Figure 1. Representation of the molecules investigated in this work.

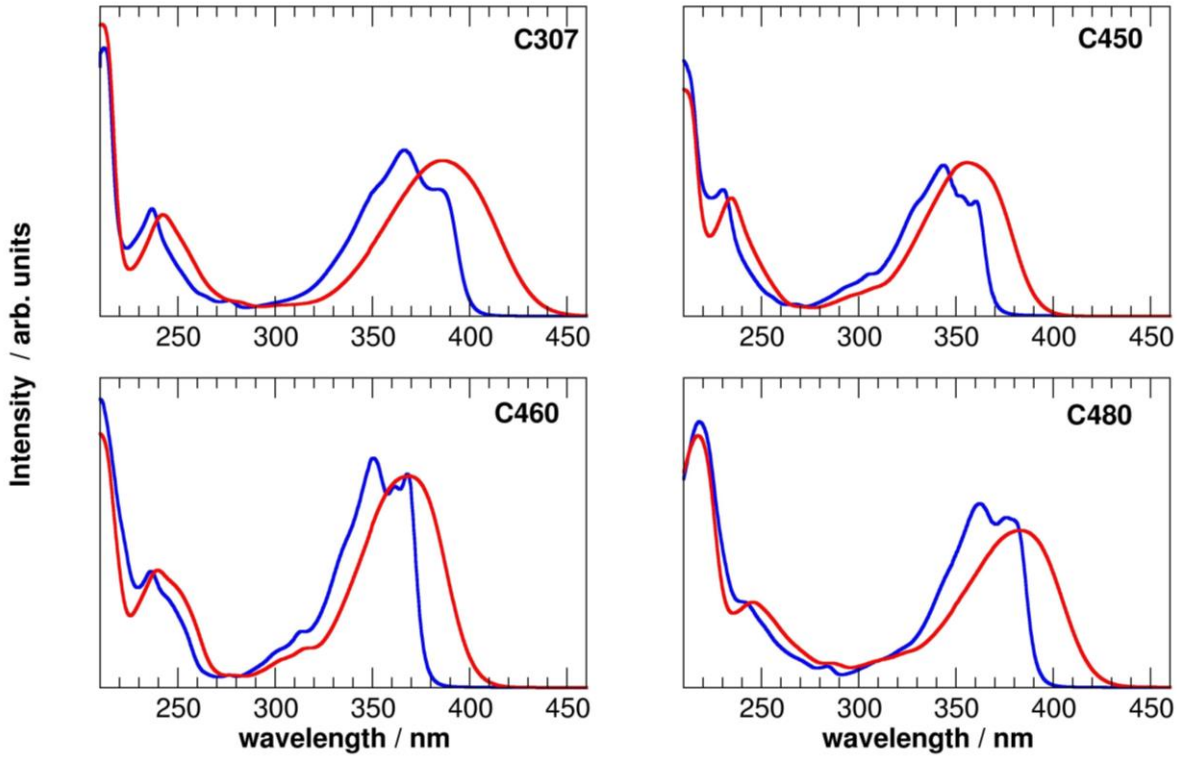

Figure 2. Experimental UV-vis absorption spectra of C307, C450, C460 and C480 in methylcyclohexane (blue) and acetonitrile (red).

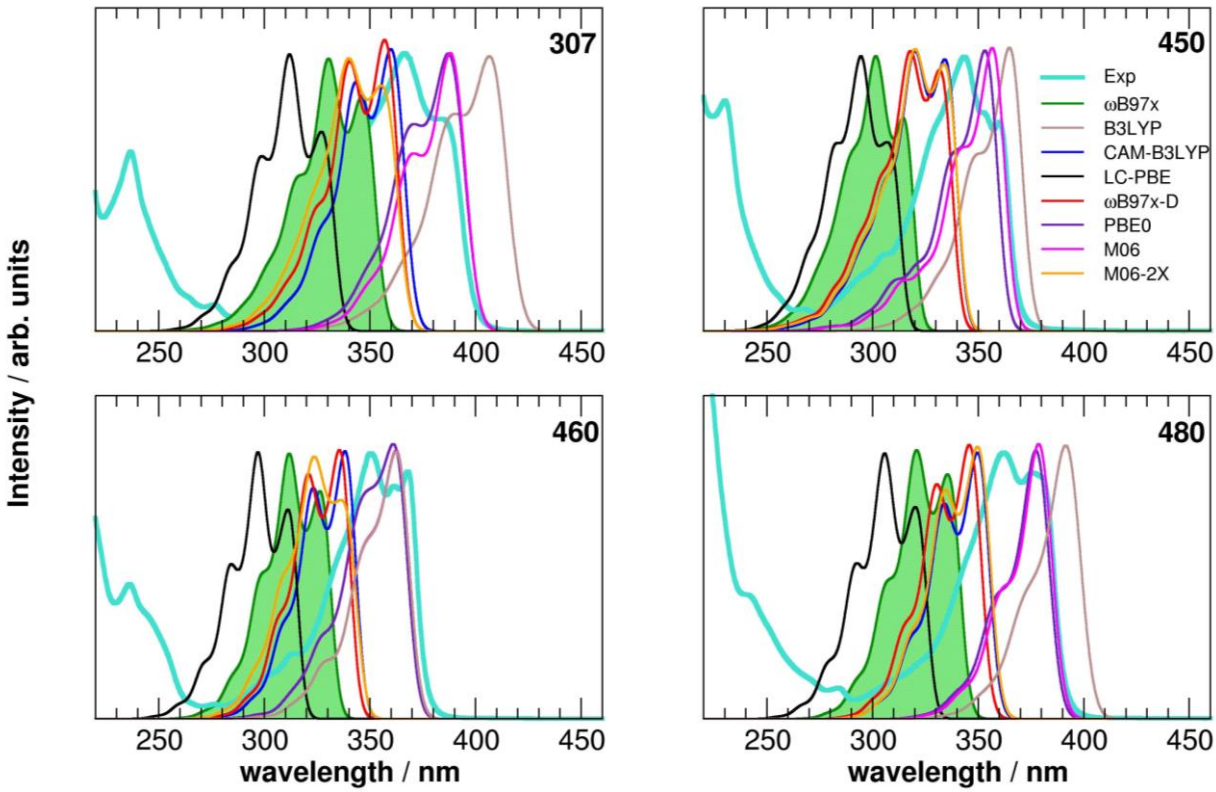

Figure 3. Comparison of the vibronic spectra of the four coumarins in methylcyclohexane computed with different exchange-correlation functionals (the experimental spectra are also reported in cyan). All vibronic calculations were performed at the AH|FC level and Gaussian distribution functions with HWHM=405 cm^{-1} were used to simulate the broadening.

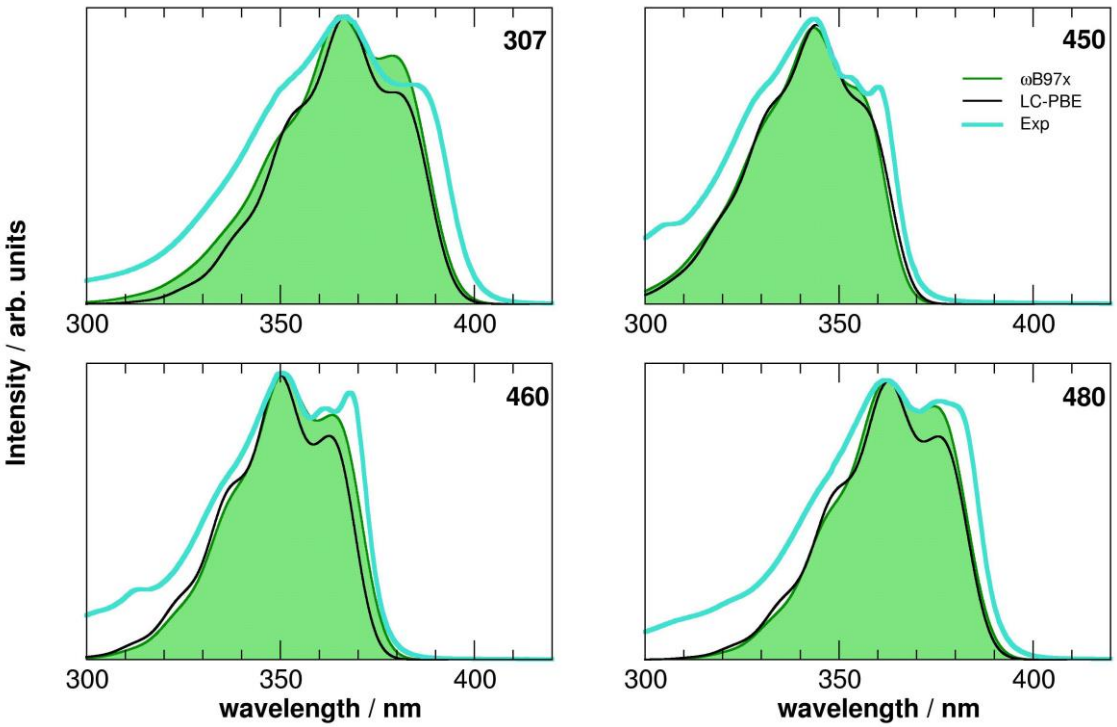

Figure 4. Comparison of the vibronic spectra of the four coumarins in methylcyclohexane computed by using LC-PBE and ωB97x exchange-correlation functionals (the experimental spectra are also reported in cyan) at 300K. All vibronic calculations were performed at the AH|FC level and Gaussian distribution functions with HWHM=540 cm^{-1} were used to simulate the broadening. Computed spectra were translated toward lower energies in order to match their maxima with the respective experimental absorption maxima.

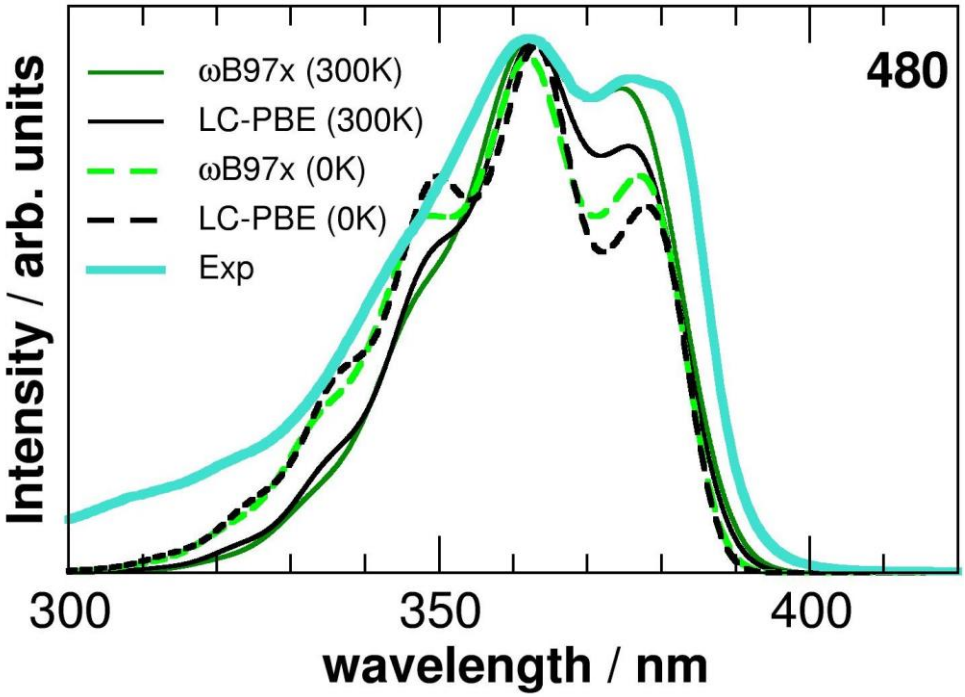

Figure 5. Comparison of the vibronic spectra of the coumarin 480 in methylcyclohexane at 0K and room temperature computed by using ωB97x and LC-PBE exchange-correlation functional (the experimental spectrum is also reported in cyan). All vibronic calculations were performed at the AH|FC level and Gaussian distribution functions with HWHM=540 cm^{-1} were used to simulate the broadening. Computed spectra were translated toward lower energies in order to match their maxima with the respective experimental absorption maxima.

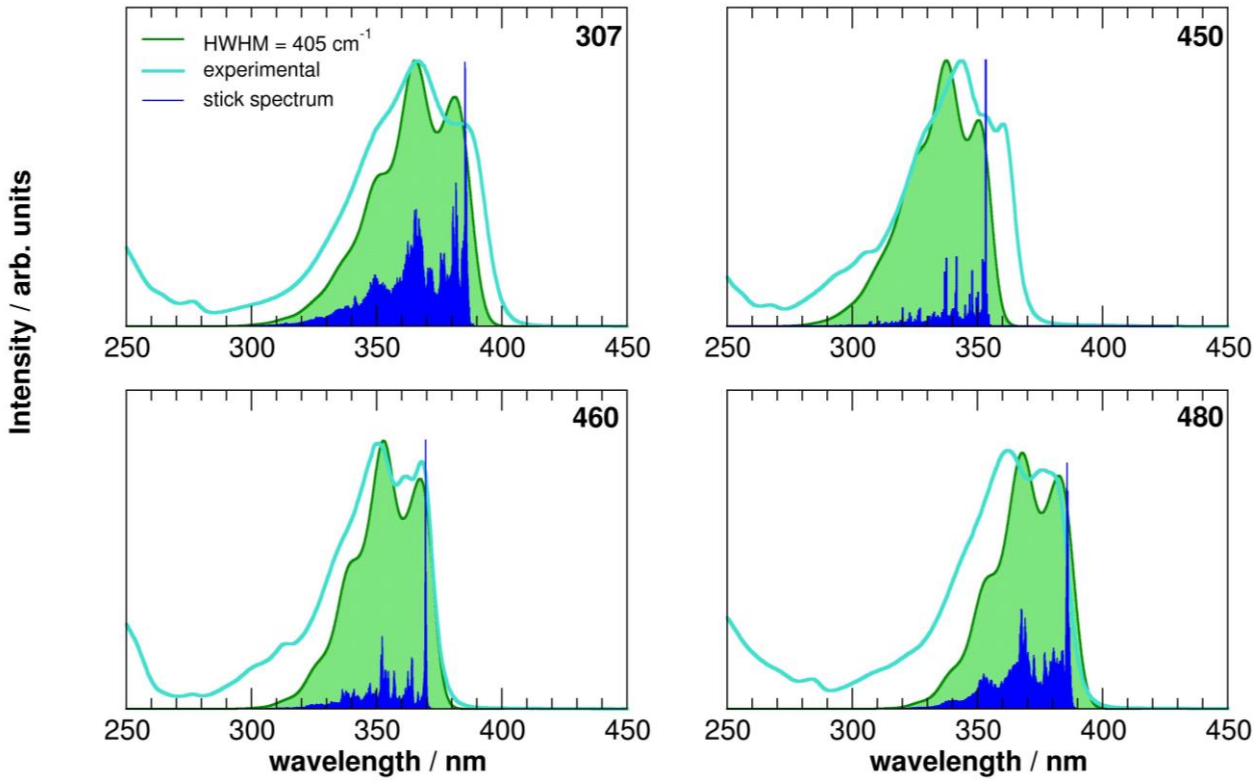

Figure 6. Comparison between the experimental spectra (red curves) and the ωB97X spectra (green curves), reported as stick and with a Gaussian broadening, and shifted by $\Delta\lambda = \lambda_{VE,PBE0} - \lambda_{VE,\omega B97X}$ = 47, 36, 41 and 47 nm for C307, C450, C460 and C480, respectively.

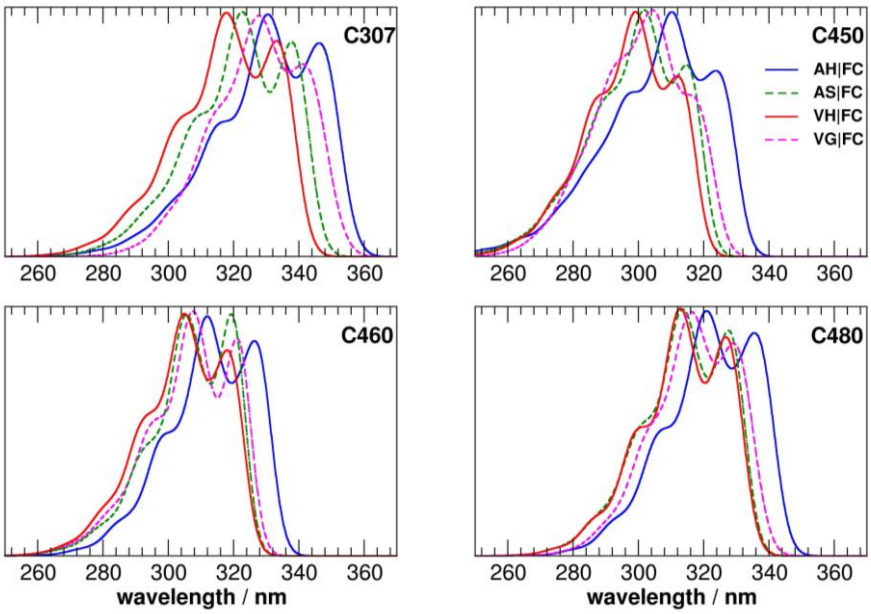

Figure 7. Vibronic spectra of C307, C450, C460 and C480 in methylcyclohexane, computed with the adiabatic hessian (AH), adiabatic shift (AS), vertical hessian (VH) and vertical gradient (VG) at the Franck-Condon level. Gaussian distribution functions with half-widths at half-maximum of 405 cm^{-1} were used to simulate the broadening.

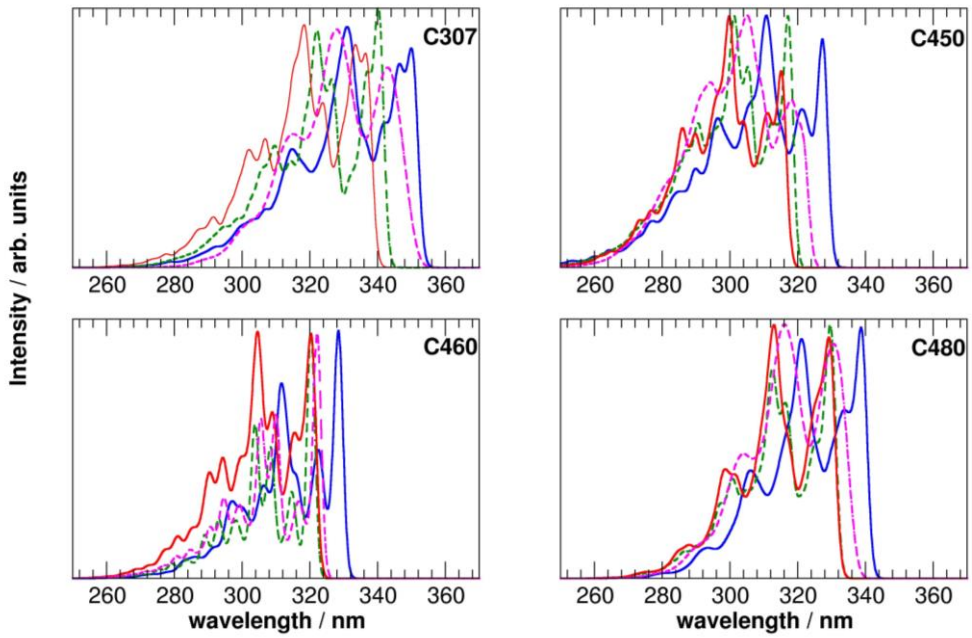

Figure 8. Vibronic spectra of C307, C450, C460 and C480 in methylcyclohexane, computed with the adiabatic hessian (AH), adiabatic shift (AS), vertical hessian (VH) and vertical gradient (VG) at the Franck-Condon level. Gaussian distribution functions with half-widths at half-maximum of 135 cm^{-1} (Gaussian default value) were used to simulate the broadening.

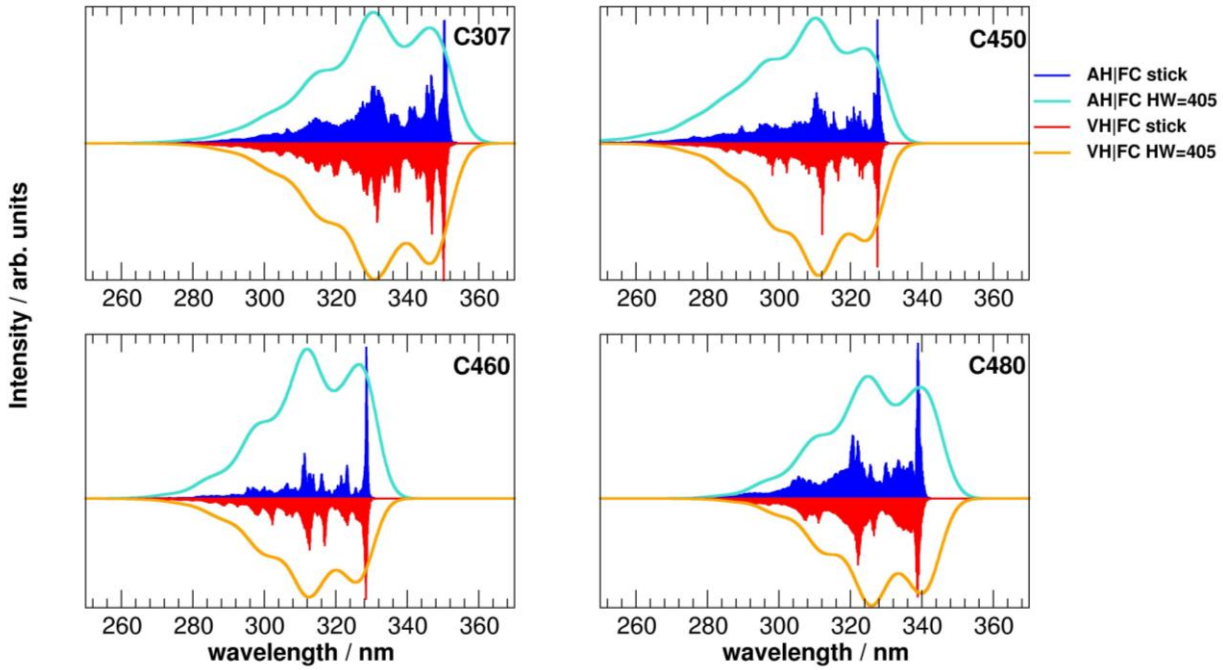

Figure 9. Vibronic spectra at T=300 K of C307, C450, C460 and C480 in methylcyclohexane, computed with the adiabatic Hessian (AH) and vertical Hessian (VH) at the Franck-Condon level. The broadening was simulated by mean of Gaussian distribution functions with half-widths at half-maximum of 405 cm^{-1}. The intensities of the VH|FC spectra were scaled by -1 to enhance the readability and shifted so that the 0-0 transition matched the one obtained with AH|FC.

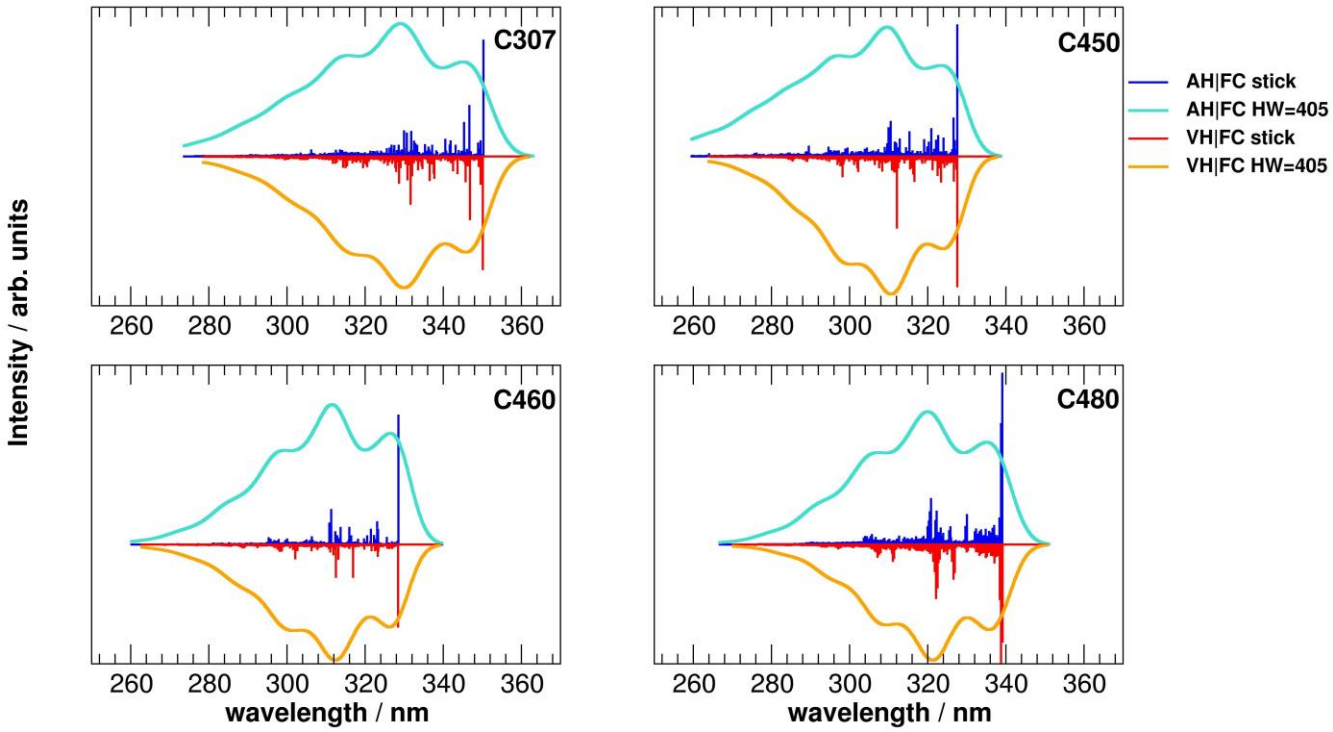

Figure 10. Vibronic spectra at 0K of C307, C450, C460 and C480 in methylcyclohexane, computed with the adiabatic Hessian (AH) and vertical Hessian (VH) at the Franck-Condon level. The broadening was simulated by mean of Gaussian distribution functions with half-widths at half-maximum of 405 cm^{-1}. The intensities of the VH|FC spectra were scaled by -1 to enhance the readability and shifted so that the 0-0 transition matched the one obtained with AH|FC.

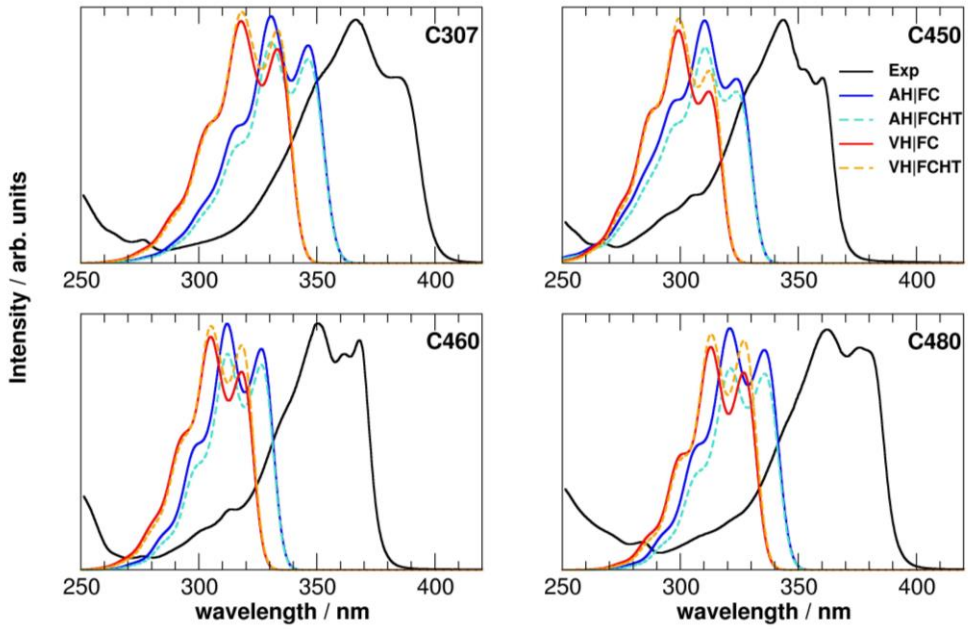

Figure 11. Vibronic spectra of C307, C450, C460 and C480 in methylcyclohexane, computed with the adiabatic Hessian (AH) and vertical Hessian (VH) at the Franck-Condon (FC) and Franck-Condon Herzberg-Teller (FCHT) levels, compared to their experimental counterparts. The broadening was simulated by mean of Gaussian distribution functions with half-widths at half-maximum of 405 cm^{-1}.

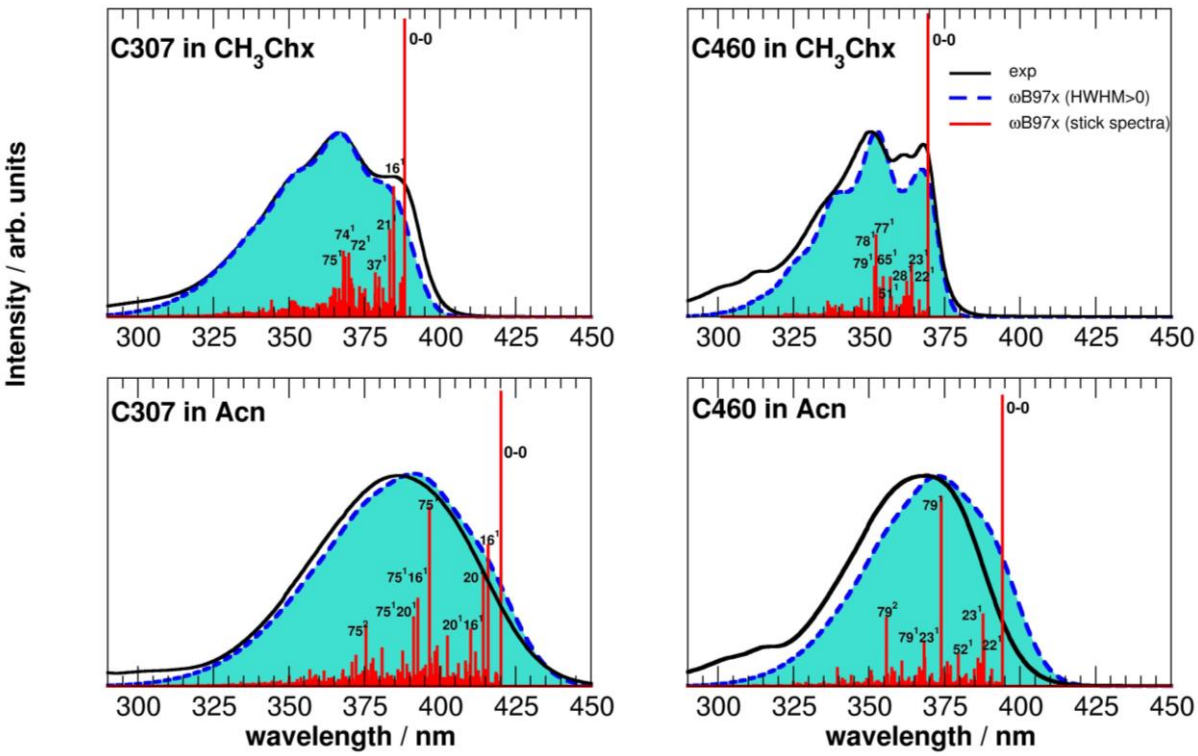

Figure 12. Computed ωB97X spectra of C307 and C460 in methyl-cyclohexane (upper panels) and acetonitrile (lower panels). For the band assignment, since all transitions are from the vibrational ground state, only the final state is indicated. The excited modes are reported with the number of quanta in superscript. Computed spectra in methyl-cyclohexane of C307 and C460 are shifted by +38 and +41 nm, respectively, in order to obtain the best match with the maxima of the experimental spectra. The computed spectra in acetonitrile are shifted by the same amounts. The broadening was simulated by mean of Gaussian distribution functions with half-widths at half-maximum of 405 (methylcyclohexane) and 800 (acetonitrile) cm^{-1}. These spectra have been computed at zero temperature.